Original Research

USPIO-Enhanced Magnetic Resonance Imaging for Nodal Staging in Patients With Head and Neck Cancer

Luís Curvo-Semedo, MD,[1] Mónica Diniz, MD,[1] Jorge Miguéis, MD,[2] Maria-José Julião, MD,[3] Paula Martins, RT,[1] Alda Pinto, RT,[1] and Filipe Caseiro-Alves, MD, PhD[1]*

Purpose: To determine the accuracy of ultrasmall superparamagnetic iron oxide (USPIO)-enhanced magnetic resonance imaging (MRI) for nodal staging in patients with head and neck cancer.

Materials and Methods: Twenty patients with carcinomas of the upper aerodigestive tract were prospectively enrolled. MRI was performed before and 24–36 hours after intravenous infusion of an USPIO agent, ferumoxtran-10 (Sinerem; Guerbet, France; and Combidex; Advanced Magnetics) at a dose of 2.6 mg Fe/kg using T2-weighted spin-echo and gradient-echo sequences. Surgery was performed the same day or the day after the ferumoxtran-10–enhanced MR examination. Based on MRI, selected nodes were surgically removed and directly correlated with pathology using hematoxylin-eosin (H&E) and Perls stainings.

Results: A total of 63 nodes were studied; 36 were nonmetastatic, 25 metastatic, and two inflammatory. Ferumoxtran-10–enhanced MRI allowed diagnosis of 24 metastatic and 30 nonmetastatic nodes, yielding a sensitivity of 96%, a specificity of 78.9%, a positive predictive value of 75%, and a negative predictive value of 96.8%, compared to 64%, 78.9%, 66.6%, and 76.9%, respectively, for nonenhanced MRI. Accuracy of ferumoxtran-10–enhanced MRI was 85.7%. The gradient-echo T2-weighted sequence was the most accurate to detect signal loss in nonmetastatic nodes.

Conclusion: USPIO-enhanced MRI is useful for nodal staging of patients with head and neck cancers.

Key Words: magnetic resonance imaging; contrast media; iron; lymphatic system; head and neck neoplasms
J. Magn. Reson. Imaging 2006;24:123–131.

CROSS-SECTIONAL IMAGING plays an important role in the study of patients with head and neck squamous cell carcinomas, allowing detection of lymph nodes (LN) missed by physical examination, or demonstrating invasion of structures such as the skull base or the carotid arteries (1,2). Using these imaging modalities, the criteria for diagnosing metastatic nodes is mainly dimensional. Measurements include the minimum transaxial diameter, the maximum transaxial diameter or a ratio between the maximum longitudinal and the maximum axial diameters (3–7). Other parameters, such as morphological criteria or the pattern of enhancement, are regarded as less important in this setting. Nodal metastases in the head and neck are frequently smaller than 10 mm, sometimes even under 5 mm in diameter, a fact that accounts for the unsatisfactory performance of the current imaging techniques (8,9).

MRI can be improved when using contrast agents suited for intravenous MR lymphography, such as the new ultrasmall superparamagnetic iron oxide (USPIO) particles, which are taken up by cells of the reticuloendothelial system of nonmetastatic LN (10–15). As it has been shown in previous studies, iron oxide deposition leads to a decrease in the signal intensity (SI) in nonmetastatic nodes due to the T2 shortening effects, whereas metastatic nodes, devoid of macrophages, will not undergo SI changes when using T2-weighted sequences (11). The clinical use of this contrast agent is still under evaluation on phase III clinical trials (15–20). Reports show promising results, with sensitivity and specificity values ranging from 59% to 100% and 77% to 100%, respectively (9,10,16,17,19,20).

The purpose of this study was to perform a direct comparison between MRI and pathological examination of selected LN in patients with head and neck cancer, determining the enhancement patterns of metastatic

[1]Department of Radiology, Hospital Universidade de Coimbra, Coimbra, Portugal.
[2]Department of Oto-rhino-laringology, Hospital Universidade de Coimbra, Coimbra, Portugal.
[3]Department of Pathology, Hospital Universidade de Coimbra, Coimbra, Portugal.
*Address reprint requests to: F.C., Department of Radiology, Hospital Universidade de Coimbra, Praceta Mota Pinto, Av. Bissaya Barreto, 3000 Coimbra, Portugal.
E-mail: fca@netvisao.pt
Received April 24, 2005; Accepted March 22, 2006.
DOI 10.1002/jmri.20602
Published online 5 June 2006 in Wiley InterScience (www.interscience.wiley.com).

and nonmetastatic nodes, and evaluating the diagnostic value of ferumoxtran-10–enhanced MRI in this group of patients. The diagnostic performance of different pulse sequences was also additionally assessed.

MATERIALS AND METHODS

Patients

This is a single-institutional study that is part of a multicentric phase III-B clinical trial, partially supported by Guerbet (Aulnay-sous-Bois, France). The ethical committee at our institution approved the study protocol, and informed written consent was obtained from all the patients enrolled. Inclusion criteria were as follows: patients of either sex, 18 years old or older (postmenopausal women or female patients with effective contraception), patients with histologically proven head and neck squamous cell carcinomas of the upper aerodigestive tract (regardless of clinical TNM stage) without previous treatment by chemotherapy and/or radiotherapy and patients scheduled to undergo surgery with bilateral lymphadenectomy within 15 days of contrast-enhanced MRI. Exclusion criteria were as follows: patients with contraindications to MRI, patients with a history of allergy to dextran or drugs containing iron salts, patients with a low-reserve hemodynamic status susceptible to decompensation after administration of contrast agent, patients who received gadolinium complexes within two days or iron oxide nanoparticles within seven days before MRI, patients who underwent previous treatment by chemotherapy and/or radiotherapy before surgery, breastfeeding female patients, patients already included in another clinical trial, patients under guardianship, and uncooperative patients.

Twenty patients were consecutively enrolled in the study, from February 2001 to October 2002. All patients were male and had a mean age of 57.3 years, with ages ranging from 39 to 78 years old. Primary tumors were located at the following regions: hypopharynx (N = 10); larynx (N = 8); and oropharynx (N = 2). The initial clinical TNM Classification of Malignant Tumours (TNM) staging based on the International Union Against Cancer (UICC) staging system classified one patient as T1, two patients as T2, 11 patients as T3, and six patients as T4. Seven patients were staged as N0, two patients as N1, 10 patients as N2, and one patient as N3.

Contrast Agent

The contrast agent ferumoxtran-10 (Sinerem, Guerbet, France; Combidex, Advanced Magnetics, USA) consists of lyophilized ultrasmall iron oxide particles (5 nm in diameter) covered with low-molecular-weight dextran. Each particle has a total diameter of approximately 30 nm. The contrast agent was reconstituted using 10 mL of a 0.9% saline solution. The administered dose was 2.6 mg of iron per kilogram of body weight. The corresponding volume of the contrast agent solution was diluted in 100 mL of a 0.9% saline solution. This final volume was injected intravenously, by drip infusion through a filter (pore size: 0.22 μm) at a rate of 4 mL/minute, with an average infusion time of approximately 30 minutes. Patients were kept under medical survey during the administration of the contrast agent and for at least two hours after completion of the infusion.

MR Imaging

All studies were performed in a 1.5-T MR magnet (Magnetom 63 SP; Siemens, Erlangen, Germany), using the Helmholtz neck coil. Images were obtained with a spin-echo (SE) proton density (PD)/T2-weighted sequence (TR: 1995 msec; TE: 25/90 msec; two acquisitions) and a gradient-echo (GRE) T2-weighted sequence (TR: 750 msec; TE: 15 msec; flip angle: 30°; two acquisitions). Both sequences were obtained in the paraaxial plane, parallel to the glottic level. Parallel presaturation bands and flow compensation pulses were routinely applied. Fifteen slices were acquired for each sequence, with a section thickness of 5 mm and an intersection gap of 0.5 mm. The field of view (FOV) was 200 × 200 mm and the matrix size was 192 (phase-encoding direction) × 256 (frequency-encoding direction) pixels, determining an in-plane pixel size of 1.04 × 0.78mm. Examinations were performed before and after intravenous administration of ferumoxtran-10. The nonenhanced examination was acquired three days before the postcontrast study. This latter examination was obtained 24 to 36 hours after the end of the ferumoxtran-10 infusion using the same imaging parameters of the nonenhanced study.

Surgical Mapping and Pathologic Correlation

Lymph nodes were selected before surgery, both by the radiologist and the surgeon, based on MRI examinations. During neck dissection, MR images were available in the surgical suite in order to properly identify the selected nodes which were removed and separately sent for pathologic examination. This analysis included measurement of the nodal diameters, followed by multiple sections of the node, with macroscopic examination of the section planes. Lymph nodes or nodal sections were included in paraffin, after fixation in a tamponated formalin solution for at least 24 hours. Sections with a thickness of 4 μm were obtained for each node or section; initially, two histology glasses from each section (or from the whole LN), were studied with standard hematoxylin and eosin (H&E) and Perls stains. The pathologist reported the nodal status on H&E stain (normal, inflammatory, or metastatic—totally or partially), the status on Perls stain (iron deposition absent or present—mild, moderate, or marked) and any important and/or uncommon histopathologic feature found. In doubtful cases, additional sections were obtained and examined. Despite the study of all LN surgically removed only those that were correlated with MRI were included for the purpose of this study.

One patient, although submitted to the post-ferumoxtran-10 examination, was excluded from the imaging and pathologic analysis, because ferumoxtran-10 infusion was prematurely stopped and not resumed, due to the appearance of facial redness, mild dyspnea, and moderate hypotension (80/50 mmHg), that disap-

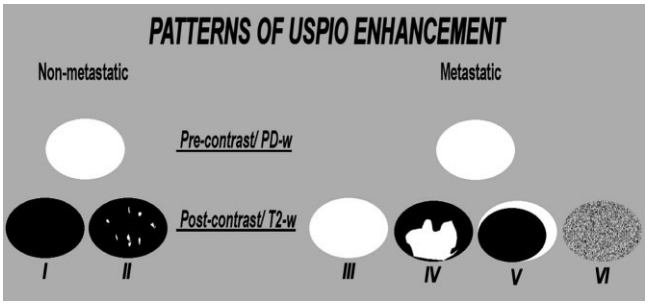

Figure 1. Drawing for visual assessment of LN SI before and after ferumoxtran-10 administration, establishing enhancement criteria used to differentiate benign from metastatic nodes. The PD-weighted images, insensitive to iron deposition, were compared to the iron-sensitive sequence (T2-weighted). LN showing a homogeneous SI decrease (*I*) on ferumoxtran-10–enhanced T2-weighted images or minute hyperintense foci (*II*) were considered nonmetastatic. Nodes that did not show SI decrease (*III*), that contained obvious foci of high SI (*IV*) or a hyperintense peripheral rim (*V*), or were heterogeneous (*VI*) on T2-weighted images in comparison to PD-weighted images were considered metastatic. The same features are applied to the evaluation of GRE T2-weighted sequences. (PD, proton density; T2-w, T2-weighted)

peared promptly after intravenous administration of methylprednisolone and saline solution. This patient received only 25% of the calculated ferumoxtran-10 dose. As a result, the efficacy was assessed on 19 patients, for a total of 63 LN being evaluated. All patients were submitted to tumor resection with bilateral radical neck dissection, with 13 having surgery the same day of the ferumoxtran-10–enhanced MR study and six one day after.

Image and Data Analysis

The MRI studies were prospectively interpreted by two radiologists (who routinely perform head and neck MR examinations), and reading results for each sequence were obtained by consensus.

The following characteristics were assessed for each selected LN: short-axis diameter (on nonenhanced MRI nodes were considered metastatic if their short axis diameter was at least equal to 10 mm), location (side and neck group, according to the nomenclature of the American Academy of Otolaryngology–Head and Neck Surgery's Committee for Head and Neck Surgery and Oncology (21)) and structure (homogeneous or heterogeneous).

On the ferumoxtran-10–enhanced examination a visual comparison of the nodal signal intensity changes was performed as three different readings (Fig. 1): in reading 1 (comparison of SI loss between ferumoxtran-10–enhanced SE PD and T2-weighted sequences), all LN that showed a SI decrease from PD to T2-weighted images were considered nonmetastatic. Nodes displaying no SI decrease, areas of high SI or a hyperintense peripheral rim on post-ferumoxtran-10 T2-weighted images in comparison to PD-weighted images were considered metastatic. In reading 2 (comparison of pre- and post-ferumoxtran-10 GRE T2-weighted sequences), nodes showing a homogeneous SI decrease in ferumoxtran-10–enhanced images in comparison to nonenhanced images or being hypointense with small and punctate hyperintense foci, were interpreted as nonmetastatic. Lymph nodes showing no SI loss compared to nonenhanced examination, containing foci of high SI or a hyperintense peripheral rim were considered metastatic. In reading 3 (comparison of ferumoxtran-10-enhanced GRE T2-weighted sequence to SI of paravertebral muscle), nodes were considered nonmetastatic if they appeared hypointense (or hypointense with punctate and scarce hyperintense foci) to paravertebral muscle. Nodes remaining iso- or hyperintense after ferumoxtran-10 administration and that showed a hyperintense peripheral rim or extensive areas of high SI were considered metastatic.

Statistical analysis was performed determining the values of sensitivity, specificity, positive predictive value, negative predictive value, and accuracy of nonenhanced and ferumoxtran-10–enhanced MRI. Accuracy between readings were analyzed using the chi squared test, with P values considered significant if <0.05.

RESULTS

Intravenous infusion of ferumoxtran-10 was well tolerated and without major side effects in 17 patients. One patient experienced mild sweating, which disappeared after few minutes without any treatment or change in the infusion protocol. In another patient, the contrast administration was momentarily interrupted due to mild hypotension that spontaneously and rapidly recovered; infusion was then carried on at a slower rate, without any further complications. In one case, the infusion was prematurely stopped and not resumed, due to the appearance of facial redness, mild dyspnea, and moderate hypotension, which subsided about 30 minutes after intravenous administration of methylprednisolone (1 g) and 0.9% saline solution. This patient was excluded from the efficacy analysis.

From the pathological study of the 19 patients submitted to cervical dissection, 821 LN were retrieved. From these 44 were metastatic (5%) and 777 were nonmetastatic (95%). From the total pool of LN, individual correlation between MRI and pathology was performed for a total of 63 nodes (average: 3.3 nodes per patient; range: 1–7 LN). Pathologic examination classified 36 (57%) as normal, 25 (40%) as metastatic (21 massively, four partially) and two (3%) as inflammatory. The nodal distribution by side, size, histologic result, and location are summarized in Tables 1 and 2.

Regarding the nodes that were subject to imaging-pathological correlation, nonmetastatic nodes had a mean short axis of 7.8 mm (range: 4–15 mm); 8 LN had a short axis equal to or larger than 10 mm. Metastatic nodes had a mean short axis length of 15.1 mm, ranging from 7 to 35 mm, with nine measuring less than 10 mm (Fig. 2).

On Perls stain, 26 normal nodes showed moderate or marked deposition of iron. In eight normal LN, there were only mild iron deposits and in another two iron was not detected. Both inflammatory nodes revealed

Table 1
Distribution of LN According to Size (Short Axis) and Location (Side)

Lymph node	Short Axis (mm)		Side
	Minimum-Maximum	Average	
Normal	4–15	7.8	24L/12R
Metastatic	7–35	15.1	11L/14R
Inflammatory	5–9	7	2L/0R

L = left, R = right.

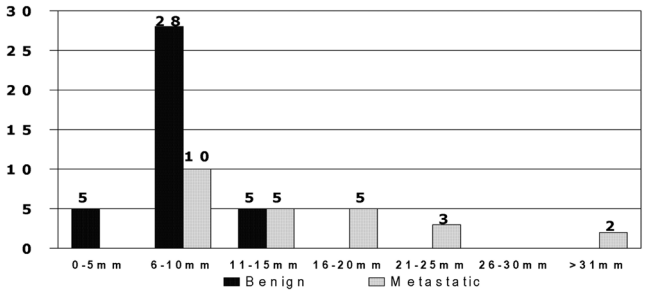

Figure 2. Distribution of benign and metastatic LN according to size (short-axis diameter). Nonmetastatic nodes tended to be smaller, whereas metastatic nodes were more variable in size.

mild iron deposition. Metastatic LN had scarce foci of iron or no iron deposits in seven and 15 cases, respectively. Two nodes showed moderate iron deposition and massive deposits were present in only one case.

In nonenhanced MRI, there were 16 true-positive and 30 true-negative LN. There were eight false-positives due to nonmetastatic nodes measuring ≥10 mm and nine false-negatives due to LN with a short axis <10 mm. Nonenhanced MRI showed a sensitivity of 64%, a specificity of 78.9%, a positive predictive value of 66.6%, and a negative predictive value of 76.9%, with an accuracy of 73%.

Regarding the results for ferumoxtran-10–enhanced MRI, in reading 1 (comparison of SI loss between SE PD and T2-weighted sequences) all 25 metastatic LN and 21 true-negative cases were identified due to absence or presence of SI loss on T2-weighted images, respectively. Seventeen LN were false positive due to the absence of a definite SI loss as reported by readers (Fig. 3). There were no false negatives; this analysis showed a high sensitivity (100%) but a low specificity (55.3%). The positive predictive value, negative predictive value, and accuracy values were 59.6%, 100% and 73%, respectively. Although ferumoxtran-10–enhanced SE PD/T2-weighted sequence was significantly more sensitive than nonenhanced MRI ($P < 0.0005$), nonenhanced MRI had a significantly better specificity ($P = 0.0089$). Readings 2 and 3 (comparison of pre- and post-ferumoxtran-10 GRE T2-weighted sequences and comparison of ferumoxtran-10–enhanced GRE T2-weighted sequence to SI of paravertebral muscle respectively) provided similar results yielding 24 true positive nodes (Fig. 4). Thirty nonmetastatic LN appeared homogeneously hypointense after ferumoxtran-10 enhancement (reading 2) or were hypointense when compared to SI of muscle (reading 3) (Fig. 3). Eight false positives were seen due to the presence of a hyperintense peripheral rim ($N = 4$) (Fig. 5) or heterogeneous SI loss compared to nonenhanced images or muscle ($N = 4$) (Fig. 6). Finally, one metastatic LN displaying a homogeneous SI decrease on post-ferumoxtran-10 GRE T2-weighted images was proved to be metastatic and thus yielded a false negative result (Fig. 7). Readings 2 and 3 provided a high sensitivity (96%) and a specificity of 78.9%. The positive predictive value was 75% and the negative predictive value was 96.8%. The diagnostic accuracy was the highest among all MRI studies (85.7%). The difference in sensitivity between nonenhanced MRI and ferumoxtran-10–enhanced GRE T2-weighted studies was highly significant ($P < 0.0005$), whereas specificity values were equivalent (78.9%; $P = 0.8341$). Specificity of readings 2 and 3 was significantly better than that of reading 1 ($P = 0.0089$), for similar sensitivity values ($P = 0.3378$). Comparison between sensitivity and specificity values regarding nonenhanced MRI and the various ferumoxtran-10–enhanced sequences are depicted in Table 3.

Table 2
Distribution of LN According to Location (Neck Levels)

Lymph nodes	Levels			
	I	II	III	IV
Normal	1	24	11	0
Metastatic	1	7	14	3
Inflammatory	0	1	1	0

On a patient-by-patient analysis, nonenhanced MRI recognized 12 true-positive patients and two true-negative patients, but erroneously classified three patients as false-positive and two as false-negative. On ferumoxtran-10–enhanced MRI all 14 metastatic patients were correctly assigned as such, but reading 1 was responsible for three false-positive results and readings 2 and 3 for two false-positives each. After ferumoxtran-10 administration there were no false-negative patients. Comparison between nonenhanced and ferumoxtran-10–enhanced MRI is showed in Table 4.

Similarly to the node-by-node analysis, ferumoxtran-10–enhanced studies improved the sensitivity and specificity regarding the nonenhanced images, identifying patients harboring metastasis with high sensitivity (100%) with the GRE T2-weighted performing better than the SE PD/T2-weighted sequence. Concerning patient management, it should be emphasized that in two patients, only the ferumoxtran-10–enhanced studies correctly assigned the presence of metastases on subcentimeter nodes.

DISCUSSION

Detection of metastatic LN in patients with head and neck cancer is extremely relevant because it is one of the most important factors influencing the prognosis; the presence of nodal metastases reduces the five-year survival to 50% regardless of the location or size of the primary tumor (17,22). Cervical palpation is inaccurate for staging purposes, since over 15% of patients clinically staged as N0 may possess nodal metastases and

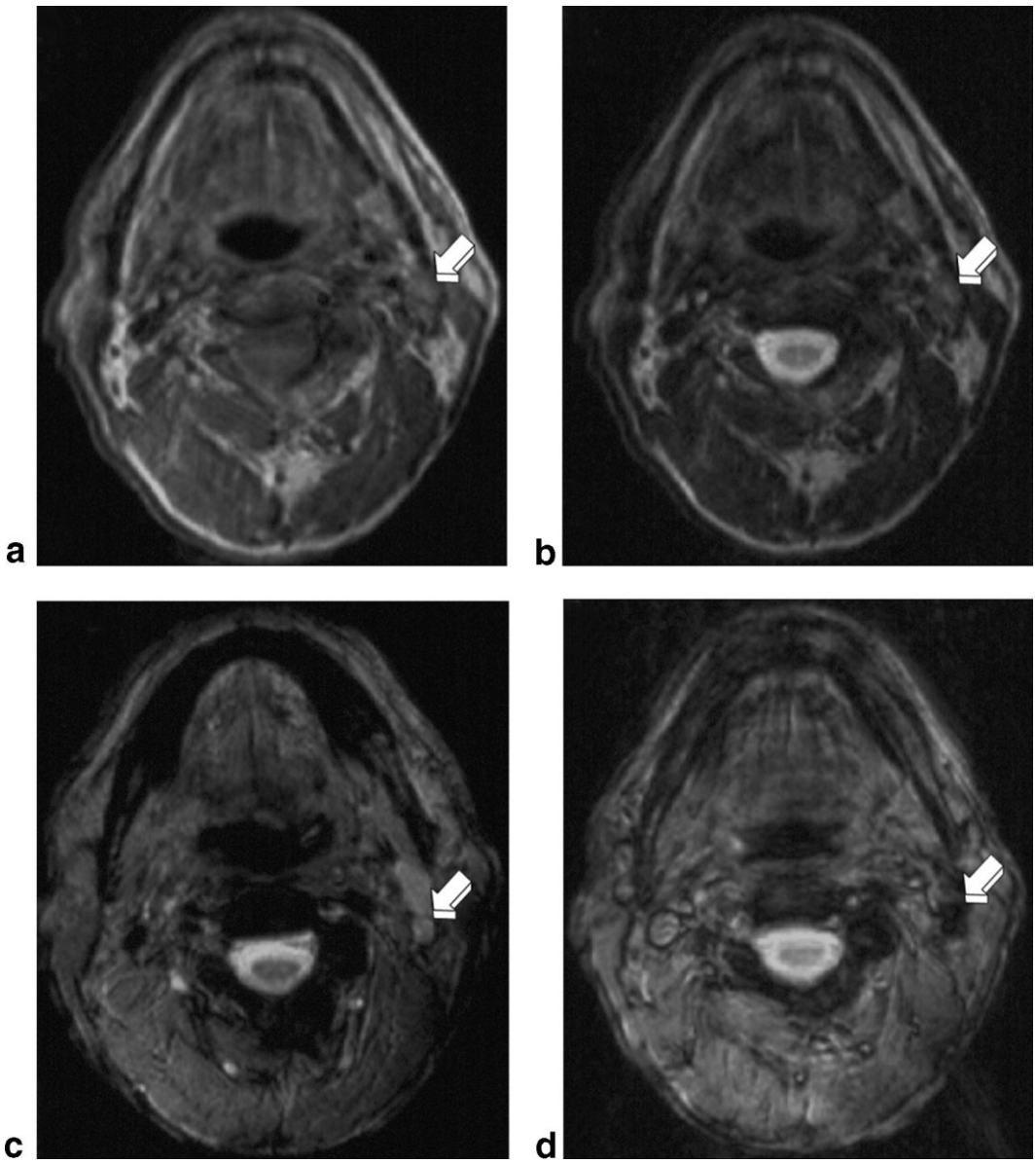

Figure 3. Normal LN. From SE PD-weighted (**a**) to SE T2-weighted images (**b**), the selected node did not reveal a clear SI loss, and thus was interpreted as metastatic. However, on the GRE T2-weighted sequence, the LN showed a clear homogeneous SI decrease from nonenhanced (**c**) to ferumoxtran-10–enhanced (**d**) images, where it appears hypointense to skeletal muscle, allowing its assignment as nonmetastatic.

rates of false-positive and false-negative cases can be as high as 15% to 25% and 30% to 50%, respectively (23,24). Due to this inaccuracy, most surgeons prefer to overtreat patients, performing bilateral radical neck dissections that may result in increased morbidity (9). Accurate presurgical imaging studies are thus needed, in an attempt to select the most appropriate surgical procedure (23). Cross-sectional imaging has been widely used in this setting and criteria for diagnosing metastatic LN include the analysis of nodal structure, clustering, shape, signs of extracapsular spread, and size (5,22,25).

MRI, with its intrinsic high soft-tissue discrimination, was thought to be a superior technique for nodal imaging, but the SI or the T2 relaxation times of metastatic nodes do not differ or even overlap those obtained in normal LN (26). Some studies did not show a clear advantage of MRI over contrast-enhanced computed tomography (CT) (27). To overcome these limitations, the use of MRI enhanced with ultrasmall iron-based contrast agents has been proposed (9–19). USPIO particles have been developed with the knowledge that they are selectively taken by cells of the reticuloendothelial system present in nonmetastatic LN, with differences in enhancement reflecting the functional status of the nodes, allowing discrimination of benign from malignant ones (17,28). Although their use for human studies has been limited (9,10,15–20), they have showed encouraging results, with reported high sensitivity and specificity values (9,10,16,17,19,20). Recently, combined positron emission tomography (PET)/CT has been used successfully for staging of nodal disease in

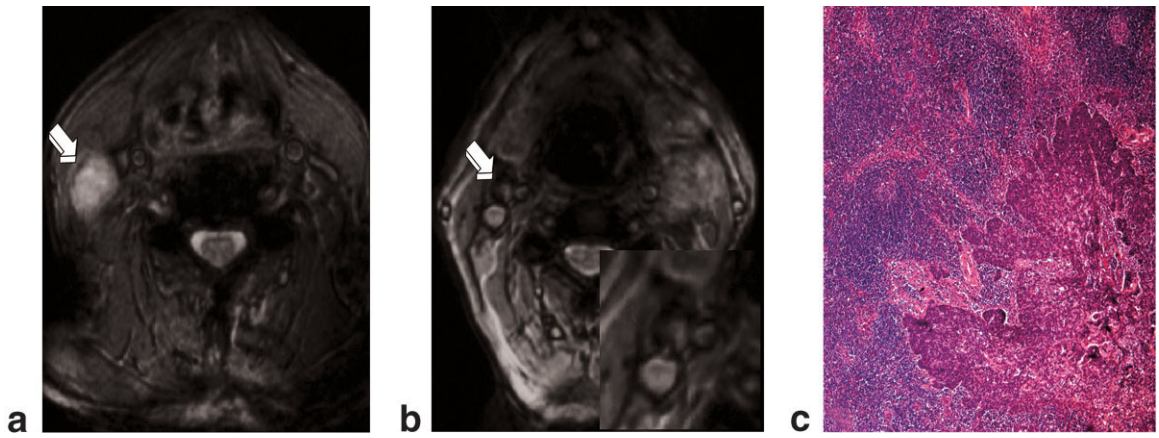

Figure 4. Metastatic LN, ferumoxtran-10–enhanced GRE T2-weighted sequence. **a:** The selected node remained hyperintense. **b:** The correlated LN showed a peripheral hypointense area and a eccentrically-located hyperintense zone (bottom right, detail); this latter area was interpreted as a partial metastasis and the pathological examination confirmed the diagnosis (H&E, 200×) (**c**).

the neck, allowing simultaneous registration of anatomic and metabolic datasets. PET/CT helps to overcome the lack of anatomical detail of isolated PET studies and may provide useful functional information for the discrimination of metastatic from nonmetastatic LN (29). To the best of our knowledge, however, at present there are no comparative studies with USPIO-enhanced MRI regarding LN status on cervical cancers.

The results of our study confirmed that using an USPIO-enhanced MRI approach it is possible to differentiate metastatic from nonmetastatic LN with a high level of accuracy, based on functional criteria and not solely on dimensional analysis. The data provided by this study reinforces those from previous works in patients with head and neck cancers, which showed a USPIO-enhanced MRI sensitivity of 95% to 96% and a specificity of 78.9% to 84% (17). More recently, Sigal et al (9), in a larger but distinct study using ferumoxtran-10 and enrolling 90 patients, reported sensitivities greater than 88% and specificities above 77%, in individual nodal analysis.

We have found a significant difference in the diagnostic performance of ferumoxtran-10–enhanced sequences, when comparing the SE PD/T2-weighted sequences and GRE T2-weighted sequences, with the latter performing better. Although the ferumoxtran-10–enhanced SE PD/T2-weighted sequences allowed detection of all metastatic nodes, they were not able to demonstrate an unequivocal SI loss in a great proportion of nonmetastatic LN, resulting in a low specificity (55.3%). On the contrary, GRE T2-weighted images allowed easier detection of nonmetastatic LN due to a more pronounced SI loss after the administration of ferumoxtran-10, providing the best contrast between areas of nonenhancement and areas of intranodal iron deposits (10,17). This is related to magnetic suscepti-

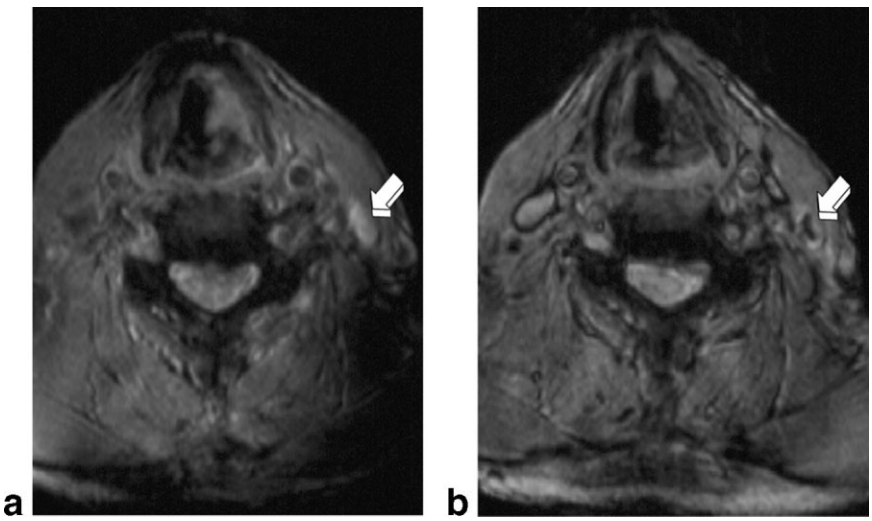

Figure 5. Normal LN measuring 6 mm of short-axis corresponding to a false-positive finding on ferumoxtran-10–enhanced GRE T2-weighted sequences. **a:** On the nonenhanced study the node is hyperintense. **b:** After ferumoxtran-10 administration there is a peripheral hyperintense rim that was thought to represent metastatic infiltration. Pathological examination found a normal histology only with a mild capsular thickening but without signs of neoplastic infiltration.

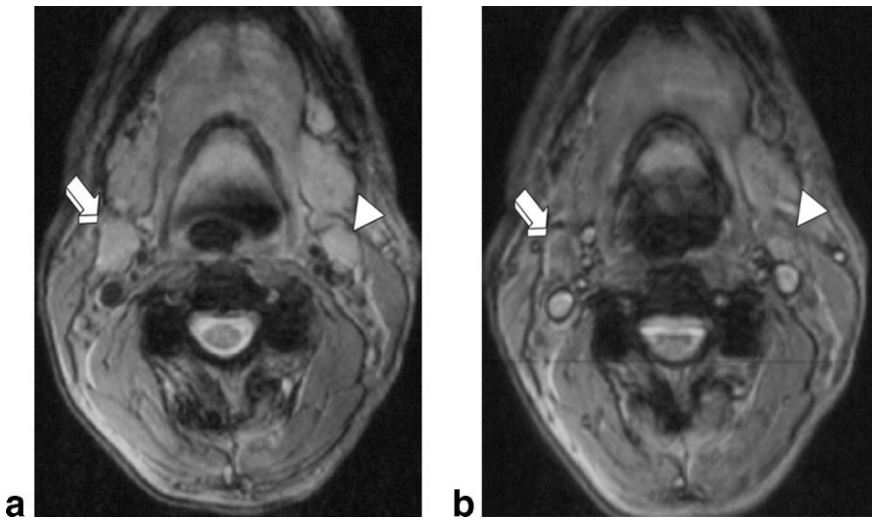

Figure 6. Nonmetastatic LN causing two cases of false-positive results using GRE T2-weighted sequences. **a:** On the nonenhanced study, the selected nodes are hyperintense. **b:** After ferumoxtran-10 enhancement, the node on the right cervical chain shows a slight heterogeneous decrease in SI (arrows). The LN on the left cervical chain also retains some hyperintense foci (arrowheads). Both were devoid of metastases on pathological examination and corresponded to inflammatory LN containing scarce focal iron deposits.

bility effects caused by the intranodal iron when using these sequences, which are deprived of the refocusing 180° pulse allowing for a greater T2-decay of tissues containing the iron oxide particles. Since the results obtained on the pre-/post-ferumoxtran-10 GRE T2-weighted sequences were identical to the analysis of the ferumoxtran-10–enhanced GRE T2-weighted sequence compared to a standard nonenhancing tissue (muscle) it seems reasonable to conclude that postcontrast images alone can be used to judge the nodal signal intensity. However, we do not provide any evidence that these results can be reproduced if reading is performed by inexperienced readers or if applied to a subset of small subcentimeter nodes. We found on ferumoxtran-10–enhanced GRE T2-weighted images eight false-positives in small nodes ≤10 mm of small axis. Four LN displayed a hyperintense peripheral rim with a central, markedly hypointense area. Pathologic examination did not reveal any particular feature except for a discrete capsular thickening but devoid of metastasis. This suggests that this pattern of nodal enhancement should also be viewed as a pattern variant for normal enhancement and not as a sign of metastatic involvement, as it was previously pointed out by Rockall et al (30) when evaluating pelvic lymph nodes in patients with gynecological cancers. Inflammatory nodes can also show a reduced uptake of USPIO due to hyperplasia of the germinal centers and paucity in macrophages as occurred in one of our cases. In the study by Sigal et al (9) false-positives resulted from inflammatory changes in the center of the nodes (hyperplastic germinal centers), with ferumoxtran-10 uptake by the macrophages only at the periphery of the LN. The same problem has also been reported in PET/CT studies, since inflammatory

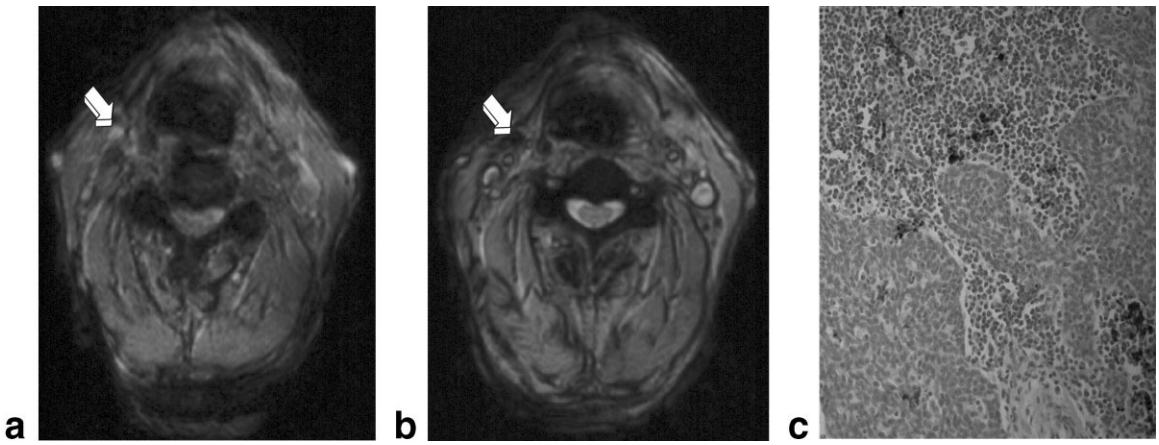

Figure 7. False-negative case after ferumoxtran-10 administration on GRE T2-weighted sequence. **a:** On the nonenhanced study, this 7-mm node was homogeneously hyperintense. **b:** After ferumoxtran-10 administration, the LN became homogeneously hypointense. **c:** Pathology was positive for metastatic involvement but marked iron deposits were also identified (Perls, 200×).

Table 3
Evaluation of LN on Nonenhanced and Ferumoxtran-10-Enhanced Sequences, Comparing to the Gold-Standard (Pathological Examination)

	Nonenhanced MRI	Ferumoxtran-10-enhanced MRI		
		SE PD/T2-w	GRE T2-w pre/post	GRE T2-w LN/muscle
Sensitivity	64% (16/25)	100% (25/25)	96% (24/25)	96% (24/25)
Specificity	78.9% (30/38)	55.3% (21/38)	78.9% (30/38)	78.9% (30/38)

SE = spin-echo, PD = proton density, T2-w = T2-weighted, GRE = gradient-echo.

changes also demonstrate an increased glucose metabolism, leading to false positive results (31). Other causes of false-positive nodes are possible and have been previously described, such as those related to the administration of lower doses of USPIO agents (17), the presence of necrosis or fatty metaplasia, a feature that can be found in about 5% of nodes (28,32). The remaining cases of false-positive results were due to a heterogeneous pattern of nodal enhancement rendering exclusion of metastasis difficult based solely on the visual appreciation of SI.

The false-negative result reported on GRE images corresponded to a 7-mm node, showing massive metastatic deposits on pathologic examination, in which the Perls stain revealed marked iron deposition. This LN did not show, however, a substantial SI loss on the SE PD/T2-weighted images and thus was correctly assigned as metastatic in reading 1. Possible explanations for this discrepancy may be related to the relatively thick slices that were obtained, and to the "blooming effect" (12,25) consisting of a strong magnetic susceptibility artifact on GRE T2-weighted sequences, obscuring nodal structure. Other false-negatives that had been described were related to the presence of micrometastases (9). The issue of intranodal micrometastases can, in fact, remain a problem since they can be present in as much as 10% of all tumor-positive specimens, with 25% of positive neck dissections containing metastases too small to be detected with the currently available imaging techniques (33). Several causes for false-negative results have also been described with PET/CT, such as a small tumor burden in metastatic nodes, nodal necrosis with a small rim of viable tumor tissue, low tracer uptake in the LN, and imaging artifacts. Nodal metastases in close vicinity to the primary tumor may also not be detectable as separate hypermetabolic foci if the latter shows very intense tracer uptake (34).

It should be stressed that in our results, all false-positives and false-negatives were seen in small nodes ≤10 mm. We think that this problem may have been amplified in our study since a high-resolution technique using phased-array coils and/or three-dimensional techniques was not available at that time in our institution. This is especially true for the GRE T2-weighted sequences, which are more prone to suffer from magnetic susceptibility artifacts and possess lower spatial resolution (35).

Our study has other limitations: the selection of the LN to be correlated was based solely in the MR image confrontation. The measurement of the nodal small axis, even if performed on iron-insensitive images, contains a certain degree of error, which may affect predominantly the precontrast study, since the criteria to declare a LN as benign or malignant are mostly dimensional. The visual analysis of the nodal SI changes, which constitutes the main judgement criterion for ferumoxtran-10–enhanced MRI, is also subjective and prone to individual variability. In our study a side-by-side or level-by-level evaluation was not performed and only the correlated resected nodes were included. We are aware that this approach carries a bias towards the selection of larger LN, possibly causing an artificial increase of sensitivity values for ferumoxtran-10–enhanced MRI because noncorrelated small metastatic nodes may be disregarded. However, since 43 (68%) of the LN selected for correlation were ≤10 mm in the short-axis (Fig. 2), the potential effects of this selection bias might have been minimized. Two patients (10.5%) received a clear benefit from ferumoxtran-10–enhanced MRI since only this technique was able to depict metastatic nodal involvement. Since all patients harboring metastatic LN at all levels were correctly identified on the ferumoxtran-10–enhanced study, the surgical decision would not been adversely affected even if we take in account the metastatic nodes that were not subjected to direct radiologic-pathological confrontation. It should be stressed that, from a clinical perspective, it is more relevant to rule out metastatic disease in a given nodal level than to determine the exact number of individual metastatic LN contained in it.

Table 4
Evaluation of Patients on Nonenhanced and Ferumoxtran-10-Enhanced Sequences, Comparing to the Gold-Standard (Pathological Examination)

	Nonenhanced MRI	Ferumoxtran-10-enhanced MRI		
		SE PD/T2-w	GRE T2-w pre/post	GRE T2-w LN/muscle
Sensitivity	85.7% (12/14)	100% (14/14)	100% (14/14)	100% (14/14)
Specificity	40% (2/5)	40% (2/5)	60% (3/5)	60% (3/5)
Accuracy	73.7% (14/19)	84.2% (16/19)	89.5% (17/19)	89.5% (17/19)

SE = spin-echo, PD = proton density, T2-w = T2-weighted, GRE = gradient-echo.

In conclusion, ferumoxtran-10–enhanced MRI improves the presurgical nodal staging of patients with head and neck cancer. The different patterns of nodal uptake in ferumoxtran-10–enhanced images must be recognized in order to avoid false results. Due to its exquisite sensitivity for the demonstration of intranodal iron deposition, GRE T2-weighted sequence should be preferred and systematically included in the imaging protocol. A single postcontrast examination may be sufficient to judge the signal intensity modification of lymph nodes if compared to an internal reference such as the nonenhancing muscular tissue.

REFERENCES

1. Sakai O, Curtin HD, Romo LV, Som PM. Lymph node pathology: benign proliferative lymphoma and metastatic disease. Radiol Clin North Am 2000;38:979–998.
2. Van der Brekel M, Castelijns J, Snow G. Diagnostic evaluation of the neck. Otolaryngol Clin North Am 1998;31:601–620.
3. Close LG, Merkel M, Vuitch MF, Reisch J, Schafer SD. Computed tomographic evaluation of regional lymph node involvement in cancer of the oral cavity and oropharynx. Head Neck 1989;11:309–317.
4. Mancuso AA, Maceri D, Rice D, Hanafee W. CT of cervical lymph node cancer. AJR Am J Roentgenol 1981;136;381–385.
5. Som PM. Lymph nodes of the neck. Radiology 1987;165:593–600.
6. Stevens MH, Harnsberger HR, Mancuso AA, Davis RK, Johnson LP, Parkin JL. Computed tomography of cervical lymph nodes: staging and management of head and neck cancer. Arch Otolaryngol 1985; 111:735–739.
7. Steinkamp HJ, Cornehl M, Hosten N, Pegios W, Vogl T, Felix R. Cervical lymphadenopathy: ratio of long-to short-axis diameter as a predictor of malignancy. Br J Radiol 1995;68:266–270.
8. Friedman M, Roberts N, Kirshenbaum GL, Colombo J. Nodal size of metastatic squamous cell carcinoma of the neck. Laryngoscope 1993;103:854–856.
9. Sigal R, Vogl T, Casselman J, et al. Lymph node metastases from head and neck squamous cell carcinoma: MR imaging with ultrasmall superparamagnetic iron oxide particles (Sinerem MR)—results of a phase-III multicenter clinical trial. Eur Radiol 2002;12:1104–1113.
10. Mack MG, Balzer JO, Straub R, Eichler K, Vogl TJ. Superparamagnetic iron oxide-enhanced MR imaging of head and neck lymph nodes. Radiology 2002;222:239–244.
11. Weissleder R, Elizondo G, Wittenberg J, Lee A, Josephson L, Brady T. Ultrasmall superparamagnetic iron oxide: an intravenous contrast agent for assessing lymph nodes with MR imaging. Radiology 1990;175;494–498.
12. Tanoura T, Bernas M, Darkazanli A, et al. MR lymphography with iron oxide compound AMI-227: studies in ferrets with filariasis. AJR Am J Roentgenol 1992;159:875–881.
13. Guimaraes R, Clement O, Bittoun J, Carnot F, Frija G. MR lymphography with superparamagnetic iron nanoparticles in rats: pathologic basis for contrast enhancement. AJR Am J Roentgenol 1994;162:201–207.
14. Lee A, Weissleder R, Brady T, Wittenberg J. Lymph nodes: microstructural anatomy at MR imaging. Radiology 1991;178:519–522.
15. McLachlan SJ, Morris MR, Lucas MA, et al. Phase I clinical evaluation of a new iron oxide MR contrast agent. J Magn Reson Imaging 1994;4:301–307.
16. Anzai Y, McLachlan SJ, Morris M, Saxton R, Lufkin R. Dextran-coated superparamagnetic iron oxide, an MR contrast agent for assessing lymph nodes in the head and neck. AJNR Am J Neuroradiol 1994;15:87–94.
17. Anzai Y, Blackwell K, Hirschowitz S, et al. Initial clinical experience with dextran-coated superparamagnetic iron oxide for detection of lymph node metastases in patients with head and neck cancer. Radiology 1994;192:709–715.
18. Harisinghani M, Saini S, Slater G, Schnall M, Rifkin M. MR imaging of pelvic lymph nodes in primary pelvic carcinoma with ultrasmall superparamagnetic iron oxide MR (Combidex): preliminary observations. J Magn Reson Imaging 1997;7:161–163.
19. Bellin M, Roy C, Kinkel K, et al. Lymph node metastases: safety and effectiveness of MR imaging with ultrasmall superparamagnetic iron oxide particles- initial clinical experience. Radiology 1998;207: 799–808.
20. Anzai Y, Piccoli CW, Outwater EK, et al. Evaluation of neck and body metastases to nodes with ferumoxtran 10-enhanced MR imaging: phase III safety and efficacy study. Radiology 2003;228:777–788.
21. Robbins KT, Medina JE, Wolfe GT, Levine PA, Sessions RB, Pruet CW. Standardizing neck dissection terminology. Official report of the Academy's Committee for Head and Neck Surgery and Oncology. Arch Otolaryngol Head Neck Surg 1991;117:601–605.
22. Som PM. Detection of metastasis in cervical lymph nodes: CT and MRI criteria and differential diagnosis. AJR Am J Roentgenol 1992; 158:961–969.
23. Johnson JT. A surgeon looks at cervical lymph nodes. Radiology 1990;175:607–610.
24. Stern WBR, Silver CE, Zeifer BA, Persky MS, Heller KS. Computed tomography of the clinically negative neck. Head Neck 1990;12: 109–113.
25. Vassallo P, Matei C, Heston W, McLachlan S, Koutcher J, Castellino R. AMI-227-enhanced MR lymphography: usefulness for differentiating reactive from tumor-bearing lymph nodes. Radiology 1994;193:501–506.
26. Dooms GC, Hricak H, Moseley MR, Bottles K, Fisher MR, Higgins CB. Characterization of lymphadenopathy by magnetic relaxation times: preliminary results. Radiology 1985;155:691–697.
27. Yousem D, Som PM, Hackney DB, Schwaibold F, Hendrix RA. Central nodal necrosis and extracapsular neoplastic spread in cervical lymph nodes: MR imaging versus CT. Radiology 1992;182: 753–759.
28. Anzai Y, Prince M. Iron oxide-enhanced MR lymphography: the evaluation of cervical lymph node metastases in head and neck cancer. J Magn Reson Imaging 1997;7:75–81.
29. Schöder H, Yeung HWD, Gonen M, Kraus D, Larson SM. Head and neck cancer: clinical usefulness and accuracy of PET/CT image fusion. Radiology 2004;231:65–72.
30. Rockall AG, Sohaib SA, Harisinghani MG, et al. Diagnostic performance of nanoparticle-enhanced magnetic resonance imaging in the diagnosis of lymph node metastases in patients with endometrial and cervical cancer. J Clin Oncol 2005;23:2813–2821.
31. Kresnik E, Mikosch P, Gallowitsch HJ, et al. Evaluation of head and neck cancer with ^{18}F-FDG PET: a comparison with conventional methods. Eur J Nucl Med 2001;28:816–821.
32. Van der Brekel MW, Stel HV, Castelijns JA, et al. Cervical lymph node metastasis: assessment of radiologic criteria. Radiology 1990; 177:379–384.
33. Van der Brekel M, van der Waal I, Meijer C, Freeman J, Castelijns J, Snow G. The incidence of micrometastases in neck dissection obtained from elective neck dissections. Laryngoscope 1996;106: 987–991.
34. Schöder H, Yeung HWD. Positron emission imaging of head and neck cancer, including thyroid carcinoma. Semin Nucl Med 2004; 34:180–197.
35. Harisinghani MG, Dixon WT, Saksena MA, et al. MR lymphangiography: imaging strategies to optimise the imaging of lymph nodes with ferumoxtran-10. Radiographics 2004;24:867–878.